Dynamic ensemble of HIV-1 RRE stem IIB reveals non-native conformations that disrupt the Rev-binding site

Chia-Chieh Chu[1], Raphael Plangger[2], Christoph Kreutz [ID][2] and Hashim M. Al-Hashimi[1,3,*]

[1]Department of Biochemistry, Duke University School of Medicine, Durham, NC 27710, USA, [2]Institute of Organic Chemistry and Center for Molecular Biosciences (CMBI), Universität Innsbruck, 6020 Innsbruck, Austria and [3]Department of Chemistry, Duke University, Durham, NC 27708, USA

ABSTRACT

The HIV-1 Rev response element (RRE) RNA element mediates the nuclear export of intron containing viral RNAs by forming an oligomeric complex with the viral protein Rev. Stem IIB and nearby stem II three-way junction nucleate oligomerization through cooperative binding of two Rev molecules. Conformational flexibility at this RRE region has been shown to be important for Rev binding. However, the nature of the flexibility has remained elusive. Here, using NMR relaxation dispersion, including a new strategy for directly observing transient conformational states in large RNAs, we find that stem IIB alone or when part of the larger RREII three-way junction robustly exists in dynamic equilibrium with non-native excited state (ES) conformations that have a combined population of ∼20%. The ESs disrupt the Rev-binding site by changing local secondary structure, and their stabilization via point substitution mutations decreases the binding affinity to the Rev arginine-rich motif (ARM) by 15- to 80-fold. The ensemble clarifies the conformational flexibility observed in stem IIB, reveals long-range conformational coupling between stem IIB and the three-way junction that may play roles in cooperative Rev binding, and also identifies non-native RRE conformational states as new targets for the development of *anti*-HIV therapeutics.

INTRODUCTION

RNAs are increasingly recognized as important regulators of gene expression (1–3), novel drug targets (4–6) and as tools for bioengineering applications and synthetic biology (7,8). RNA and other biomolecules do not fold into a single structure but rather form a statistical ensemble of many interconverting conformations (9–12). The biological activities of nearly all non-coding RNAs depend on these dynamics. For example, binding of ligands, proteins other RNAs, or changes in physiological conditions such as temperature can favor specific conformations in the ensemble and cause a structure-specific change in activity (13–15). Thus, a deep understanding of how RNAs function within cells requires an understanding of their dynamic behavior. This in turn may enable the targeting of RNA in drug discovery efforts (12,13) as well as the rational design of RNA-based devices (7).

Application of different biophysical techniques have led to certain themes that reoccur in the ensemble description of RNA (15). One theme is that many RNAs transiently form alternative conformations *in vitro* and *in vivo* that feature non-native secondary structure (9,16–20). These alternative conformations, often referred to as 'excited states' (ESs) (16,17,21), form on the micro-to-millisecond timescale and involve small differences in base-pairing in and around non-canonical motifs such as bulges and internal loops. These dynamic transitions can serve as facile switches (22,23) or help break down larger conformational transitions into multiple kinetically labile microscopic steps (18,24,25). Given the growing observation of such non-native conformations in a variety of RNAs by NMR (26–28) and chemical probing (29–31), it is important to examine their biological roles and their potential as new drug targets, and to assess how they might impact the interpretation of mutagenesis and structure probing data *in vitro* and *in vivo*.

The Rev response element (RRE) from the human immunodeficiency virus type 1 (HIV-1) (32–35) is an example of a flexible RNA drug target (36–41) and has the potential to adopt such alternative non-native conformations (42–44). RRE is a ∼350 nt *cis*-acting RNA element lo-

*To whom correspondence should be addressed. Tel: +1 919 660 1113; Fax +1 919 684 8885; Email: hashim.al.hashimi@duke.edu

cated within the *env* gene (32–34). In HIV-1, RRE mediates export of unspliced or partially spliced viral RNAs to the cytoplasm by coordinating the assembly of multiple molecules of the viral protein Rev to form a homo-oligomeric ribonucleoprotein complex (35,45–48). The assembly of this complex has been the subject of many investigations (42,49–53). RRE folds into a structured RNA with five distinct stem loops (I–V) (46,54,55). Studies indicate that two Rev molecules bind cooperatively to high affinity sites in stem IIB and the nearby stem II three-way junction (42,48,49,56,57) (Figure 1A). This initial binding event is thought to nucleate assembly, which then extends to stem I, including a high affinity site in stem IA, ultimately resulting in the coordinated and sequential binding of multiple Rev copies through a series of Rev–Rev and Rev–RRE interactions (35,42,48,52). The high concentration of Rev required for assembly is thought to set an expression threshold such that Rev would only function during later stages of viral replication (35,45).

Because of its central importance in viral mRNA export and HIV replication (32,58–61), stem IIB has been the subject of numerous biochemical and structural studies including efforts to target RRE in the development of anti-HIV therapeutics (36–40). NMR and X-ray structures of isolated stem IIB in complex with Rev arginine-rich motif (ARM) show that RNA recognition leads to conformational changes; G71 transitions from a *syn* to *anti* conformation forming a trans G48(*anti*)-G71(*anti*) mismatch, and binding stabilizes the Watson–Crick:Watson–Crick G47(*anti*)–A73(*anti*) mismatch. These conformational changes serve to widen the major groove to accommodate binding of ARM as an α-helix that forms base-specific hydrogen bonds and electrostatic interactions with backbone phosphate groups (43,44,56,62–66). Biochemical studies show that an additional Rev molecule binds cooperatively at the nearby stem II three-way junction (45,48,67). A recent crystal structure of stem IIB containing an engineered junction site with a Rev dimer shows that the junction site helps orient the Rev subunits through interactions that depend on the junction architecture (56). Biochemical studies indicate that flexibility at the junction is important for adaptive recognition of the second Rev molecule through non-specific interactions and is also an important determinant of binding affinity and cooperativity (48,49,68). Indeed, the high SHAPE reactivity observed for nucleotides within stem IIB and the stem II three-way junction within the larger ~234 and ~354 nt RRE contexts indicates that this region is highly flexible. NMR studies of isolated stem IIB also provide evidence for flexibility in the purine-rich region (43,44). However, the nature of this flexibility has remained elusive.

In this study, we used NMR relaxation dispersion (RD) techniques to examine the dynamics of RRE stem IIB in isolation and when part of the three-way junction. The data indicate that stem IIB forms a dynamic ensemble of three conformations including two non-native ESs that remodel key structural elements required for Rev binding. We discuss potential roles for the ESs in cooperative Rev binding and propose that they provide new targets for the development of anti-HIV therapeutics.

MATERIALS AND METHODS

Preparation of RNA samples

RREIIB, RREII and mutants (A68C-RREIIB, U72C-RREIIB, A68C-RREII, U72C-RREII and A68C/G50A/C69U-RREII) were prepared by *in vitro* transcription using T7 RNA polymerase (New England Biolabs Inc.), chemically synthesized DNA templates (Integrated DNA Technologies) with designed T7 promoter sequence (TTAATACGACTCACTATA) and uniformly $^{13}C/^{15}N$-labeled nucleotides triphosphates (Cambridge Isotope Laboratories Inc.). RREIIB mutants (UUCG-RRE20, UUCG-G48A/G50U and m^3U72-RREIIB) were synthesized using an in-house oligo synthesizer (MerMade 6, BioAutomation) with solid-phase RNA synthesis using N-acetyl protected 2′-tBDSilyl-phosphoramidites (Chem-Genes Corporation) and 1 μmol standard columns (1000 Å, BioAutomation) with 4,4′-dimethoxytrityl (DMT)-off synthesis followed by base and 2′-O deprotection (100 μmol DMSO, 125 μl TEA•3HF) and ethanol precipitation. The DMT-off 2′-O deprotection is recommended for larger RNA synthesis to obtain cleaner NMR spectra.

A similar approach was used to synthesize site-labeled $^{15}N3$-U72-RREII, $^{13}C6$-U72-RREII and $^{13}C8$-G71-RREII using $^{15}N3$-uridine phosphoramidites, $^{13}C6$-uridine phosphoramidites and $^{13}C8$-guanosine phosphoramidites, respectively (69). All RNA samples were purified using 20% (w/v) denaturing polyacrylamide (29:1) gel within 8 M urea, 20 mM Tris Borate and 1 mM ethylene-diaminetetraacetate (EDTA) TBE buffer followed by Elutrap electro-elution system (Whatmann, GE healthcare) with 40 mM Tris acetate and 1 mM EDTA (TAE) buffer then ethanol precipitation. The RNA pellets were dissolved in water and annealed by heating at 95°C for 10 min then rapidly cooling on ice. After measuring the concentration, the RNA samples were concentrated and buffer-exchanged with 10× buffer volume three times (NMR buffer: 15 mM sodium phosphate, 25 mM NaCl, 0.1 mM EDTA, with or without 3 mM $MgCl_2$ at pH = 6.4) using Amicon Ultra centrifugal filters (EMD Millipore). When changing pH, the final pH of the NMR sample was verified to be identical to that of the buffer. For NMR samples in 100% D_2O, the RNA samples were flash frozen and lyophilized overnight before dissolving in 100% D_2O (EMD Millipore).

NMR experiments

Resonance assignment. NMR experiments were performed on Bruker Avance III 600-MHz or 700 MHz-NMR spectrometers equipped with 5 mm triple-resonance cryogenic probe at 10 or 25°C. The RREIIB resonances in 2D $^1H,^{15}N$ (N1/N3-H1/H3) and $^1H,^{13}C$ (C2/C6/C8-H2/H6/H8) heteronuclear single quantum coherence (HSQC) spectra were assigned using 2D ^1H-^1H nuclear overhauser effect spectroscopy (NOESY) with 180 ms mixing time for exchangeable proton at 10°C with 10% D_2O and 220 ms mixing time for non-exchangeable proton at 37°C in 100% D_2O in the absence of Mg^{2+} using 1.0–1.2 mM $^{13}C/^{15}N$-uniformly labeled RNA samples in NMR buffer (15 mM sodium phosphate, 25 mM NaCl, 0.1 mM
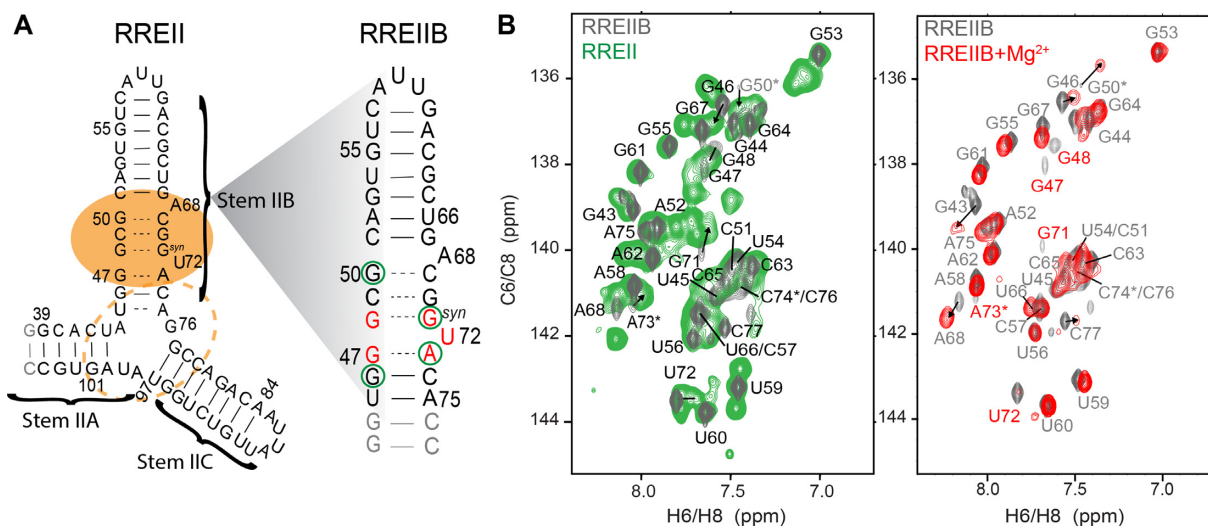
Figure 1. RRE constructs used in NMR studies. (**A**) Three-way junction (RREII) and stem IIB (RREIIB) constructs used in this study. The Rev primary and secondary binding sites are indicated using filled and dashed orange circles, respectively. Base pairs with and without detectable H-bonds are indicated using solid and dashed lines, respectively. Residues showing differences in chemical shifts between RREII and RREIIB or that have broadened resonances indicative of micro-to-millisecond exchange are highlighted using green circles and colored red on RREIIB, respectively. (**B**) Comparison of aromatic 2D ^{1}H,^{13}C-HSQC of RREIIB (black) with RREII (green) and RREIIB plus Mg^{2+} (red). The sample conditions were 1.0–1.2 mM RREII or RREIIB in 15 mM sodium phosphate, 25 mM NaCl, 0.1 mM EDTA, pH 6.4 with or without 3 mM MgCl$_2$. Resonances exhibiting line-broadening are labeled in red and those with ambiguous assignments denoted using an asterisk.

EDTA, pH 6.4). The same HSQC and NOESY (mixing time 180 ms) experiments were used to assign resonances in UUCG-RRE20 and UUCG-G48A/G50U RRE mutants at 25°C in the absence of Mg^{2+} using 1.8–2.0 mM RNA samples in NMR buffer (15 mM sodium phosphate, 25 mM NaCl, 0.1 mM EDTA, pH 6.4) with 10% D$_2$O. All NMR data were analyzed using NMRPipe (70) and SPARKY (T.D. Goddard and D.G. Kneller, SPARKY 3, University of California, San Francisco).

R $_{1\rho}$ measurements. ^{13}C RD experiments (71,72) were carried out on Bruker Avance III 700-MHz NMR spectrometer with 5-mm triple-resonance cryogenic probe at 25°C using 1.0–1.2 mM ^{13}C/^{15}N-uniformly labeled RNA samples in NMR buffer (15 mM sodium phosphate, 25 mM NaCl, 0.1 mM EDTA, pH 6.4 with or without 3 mM Mg^{2+}). On- and off-resonance RD data on aromatic (C8, C6) spins were measured with varying spinlock powers ($\omega 2\pi^{-1}$ Hz) and off-sets ($\Omega 2\pi^{-1}$ Hz) (Supplementary Table S2) using seven delay times between 0 and 60 ms (73). Peak intensities for each delay time point were obtained using NMR-Pipe and fit to a monoexponential decay function using in-house python script to calculate $R_{1\rho}$ values (74). Errors in $R_{1\rho}$ were estimated using Monte Carlo simulations with 500 iterations as previously described (75).

R $_{1\rho}$ data analysis. The RD data were analyzed to obtain exchange parameters through numerical solutions of the Bloch-McConnell equations (21) using an in-house python script (74). The data were fit using two-state (individual or global) or three-state (individual or global) models with or without minor exchange using average effective field alignment as previously described (17,74). Global fitting of the data was carried out by sharing the populations and k_{ex} of ES1 and ES2 (Supplementary Table S1). Model selec-

tion was preformed as previously described (23) using the Akaike's (w_{AIC}) and Bayesian information criterion (w_{BIC}) weights to select the model with the highest relative probability (76,77).

Fluorescence anisotropy binding experiments

Binding experiment was preformed using a Rev-ARM peptide labeled with 3′-end fluorescein (Rev-Fl, TRQARRNRRRRWRERQRAAAACK-FITC, LifeTein LLC) (78). Fluorescence anisotropy measurements were performed using a CLARIOstar plate reader (BMG LABTECH) using 480 nm excitation and 540 nm emission filter. A constant concentration of Rev-Fl (1 nM for RREIIB and RREII mutants, 10 nM for other constructs) was added into 384-well plate with serially diluted RNA in the reaction buffer (30 mM HEPES, pH = 7.0, 100 mM KCl, 10 mM sodium phosphate, 10 mM ammonium acetate, 10 mM guanidinium chloride, 2 mM MgCl$_2$, 20 mM NaCl, 0.5 mM EDTA and 0.001% (v/v) Triton-X100) (78). K_d values were obtained by fitting the measured fluorescence anisotropy values to one-site binding equations using least-squares methods implemented in Mathematica 10.0 (Wolfram Research).

$$A = A_{\text{free}} + (A_{\text{bound}} - A_{\text{free}})$$

$$\times \left[\frac{R_T + L_T + K_d - \sqrt{(R_T + L_T + K_d)^2 - 4 R_T * L_T}}{2 R_T} \right]$$

A is the measured value of fluorescence anisotropy; R_T is the total RNA concentration; L_T is the total Rev-Fl concentration; A_{free} is the anisotropy without Rev-Fl binding; A_{bound} is the anisotropy with saturated Rev-Fl binding; and K_d is the dissociation constant. The uncertainty in the fluorescence anisotropy was obtained based on the standard deviation over triplicate measurements.

RESULTS

Mg²⁺ and the three-way junction impact the structural dynamics of stem IIB

Prior NMR studies were conducted in the absence of Mg²⁺ and focused exclusively on isolated stem IIB in which the stem II three-way junction was omitted and replaced with stable base pairs (43,44,62–64). However, considering the close proximity of stem IIB to the three-way junction, it is possible that such isolated constructs of stem IIB in the absence of Mg²⁺ do not fully capture the structural dynamics in the biologically relevant three-way junction context in the presence of Mg²⁺. We therefore used NMR to compare an isolated 35 nt construct of stem IIB (RREIIB) with a 68 nt construct (RREII) containing the stem II three-way junction (Figure 1A). Both constructs avoid mutations used in prior NMR and X-ray studies of RREIIB (43,44,56,65,66). 2D ¹H,¹³C-HSQC spectra of RREIIB in the absence of Mg²⁺ revealed that many resonances in the internal loop (G47 to G50 and A68 to A73) are significantly broadened (Figure 1B and Supplementary Figure S1). This was the first hint that stem IIB undergoes micro-to-millisecond timescale exchange with alternative ES conformations. Addition of 3 mM Mg²⁺ resulted in small chemical shift perturbations indicating minor changes in the dominant ground state (GS) structure (Figure 1B and Supplementary Figure S2). In addition, Mg²⁺ further broadened resonances belonging to nucleotides in the purine-rich internal loop (G47, G48, G71, U72, A73), indicating increased micro-to-millisecond conformational exchange, whereas it reduced the broadening at the A68 bulge, indicating a decrease in micro-to-millisecond exchange (Figure 1B and Supplementary Figure S2). Analysis of NOE distance-based connectivity and chemical shifts measured in RREIIB suggests a dominant GS conformation similar to that reported in prior NMR studies (43,44) with G48(*anti*)–G71(*syn*) and G47(*anti*)–A73(*anti*) mismatches, partially stacked A68 bulge, and flipped out U72 bulge (Figure 1B and Supplementary Figure S1). The G48(*anti*)–G71(*syn*) mismatch could adopt either Watson–Crick:Watson–Crick or Watson–Crick:Hoogsteen pairing and both conformations have been reported in prior NMR (63) and X-ray (65,66) structures of RRE. However, the lack of observable imino and amino signals particularly in these WT RRE sequences makes it difficult to distinguish these different pairing modes. Likewise, the G47(*anti*)–A73(*anti*) mismatch could form either Watson–Crick:Watson–Crick or sheared mismatch, but again these are difficult to distinguish due lack of observable G47 imino and amino resonances and A73 C2H2.

We find very good agreement when overlaying spectra of RREIIB with those of the RREII three-way junction both in the absence or presence of Mg²⁺ (Figure 1B; Supplementary Figures S1 and S2). However, small differences are observed for G46 near the three-way junction and more distant residues such as G71 and G50 (Figure 1B and Supplementary Figure S1B). These perturbations most likely reflect changes in the GS ensemble possibly due to transient stacking interactions with the different stems in the three-way junction. While we do not observe any imino ¹H NOE

connectivity between the helices, the junctional base pairs of all three stems form with detectable imino protons, i.e. they are relatively stable (Supplementary Figure S1). Thus, we cannot rule out that some of the stems are at least transiently stacked in the three-way junction. In addition, the line broadening at the purine rich region was more severe in RREII as compared to RREIIB in both the absence and presence of Mg²⁺ (Supplementary Figures S1 and S2). These results indicate that the three-way junction and Mg²⁺ have small effects on the stem IIB GS conformational ensemble as well as on micro-to-millisecond conformational exchange with ESs.

Characterizing conformational exchange using NMR relaxation dispersion

To gain further insights into the conformational exchange, we carried out using $R_{1\rho}$ RD NMR experiments on RREIIB both in the presence and absence of Mg²⁺. The $R_{1\rho}$ experiment (71,79) measures the chemical exchange contribution (R_{ex}) to intrinsic transverse relaxation rate ($R_{2,int}$) of NMR resonances during a relaxation period, when the spin is irradiated with an applied radiofrequency pulse with varying powers ($\omega 2\pi^{-1}$) and frequencies ($\Omega 2\pi^{-1}$).

In the absence of Mg²⁺, RD consistent with micro-to-millisecond exchange was observed for most residues in the Rev-binding site (G46-C8, G47-C8, G67-C8, A68-C8, G71-C8, U72-C6) (Figure 2A). In contrast, no RD was observed for residues outside this region (A52-C8, G53-C8, U66-C6 and A75-C8) (Figure 2A). Similar nucleotide specific RD was observed in the presence of 3 mM Mg²⁺ though the lower quality of the NMR spectra did not permit RD measurements for all residues (Supplementary Figure S2). However, the RD profiles differed in Mg²⁺ and were enhanced for U72-C6 while they were diminished for A68-C8 (Figure 2B), consistent with the Mg²⁺-induced changes in line-broadening observed in 2D ¹H,¹³C-HSQC spectra (Supplementary Figure S2).

Fitting of the RD data (see 'Materials and Methods' section) allowed determination of the ES population (pᴮ), the exchange rate ($k_{ex} = k_1 + k_{-1}$) and the carbon chemical shift differences between the GS and ES ($\Delta \omega = \omega_{ES} - \omega_{GS}$), which carry information regarding the ES conformation (80). Most RD data could be satisfactorily fit to a two-state (GS ⇌ ES) model (Figure 2B and C; Supplementary Figure S3A). However, for U72-C6, G71-C8, G46-C8 and G47-C8 (Figure 2B and C; Supplementary Figure S3A), the asymmetric RD profiles called for a three-state (ES1 ⇌ GS ⇌ ES2) fit with star-like topology (Figure 3A) (17,80). The RD data therefore indicate that in RREIIB, stem IIB transiently forms at least two distinct ES conformations both in the presence and absence of Mg²⁺ (Supplementary Table S1).

Global fitting of the RD data (see 'Materials and methods' section) indicates that in the presence of Mg²⁺, ES1 is highly abundant with pᴮ ∼18% and exchange rate $k_{ex} \sim 6195$ s⁻¹ that is fast on the NMR timescale (Supplementary Figure S3B and Supplementary Table S1). Its formation involves changes in G46, G47, G71 and U72 in the lower internal loop (Figure 2A). Relative to ES1, ES2 has a lower abundance with $p_B \sim 4\%$ and comparable exchange rate with $k_{ex} \sim 2364$ s⁻¹. Its formation involves changes in G46
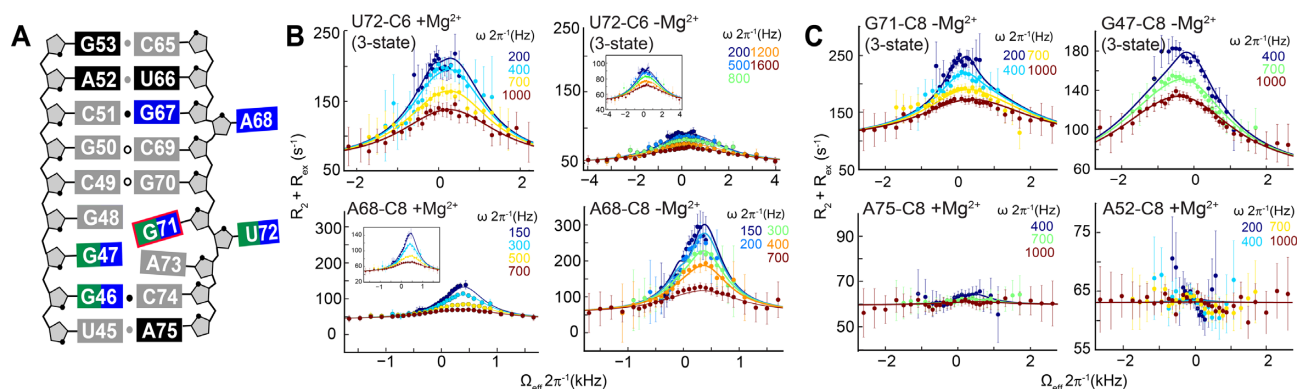
Figure 2. Off-resonance $R_{1\rho}$ NMR measurements in RREIIB. (**A**) Secondary structure of RREIIB. Nucleotides with no RD, ES1 and/or ES2-specific RD are colored black, green and blue, respectively. Nucleotides for which RD could not be measured are in gray. *Syn* base is indicated with the red box. (**B**) Comparison of off-resonance $R_{1\rho}$ profiles in the presence and absence of 3 mM Mg^{2+}. Different power levels ($\omega 2\pi^{-1}$) are color-coded. Solid lines represent the global fits to the RD data. Error bars represent experimental uncertainty based on Monte Carlo analysis of monoexponential decay curves and the signal noise. (**C**) Representative examples of off-resonance $R_{1\rho}$ profiles showing resonances with three-state RD and absence of RD. The sample conditions were 1.0–1.2 mM RREIIB in 15 mM sodium phosphate, 25 mM NaCl, 0.1 mM EDTA, pH 6.4 with or without 3 mM $MgCl_2$.

and U72 at the lower internal loop as well as A68 and G67 in and above the internal loop (Figure 2A). While the similar $\Delta\omega$ values indicate that Mg^{2+} does not alter the ES conformation (Supplementary Figure S3C), the ES1 population decreased 3-fold in the absence of Mg^{2+} ($p_B = 5.7\%$ and $k_{ex} = 10751$ s^{-1}) while that of ES2 increased ∼3-fold ($p_B = 11\%$ and $k_{ex} = 2311$ s^{-1}) (Supplementary Figure S3B and Supplementary Table S1). Thus, Mg^{2+} preferentially stabilizes ES1 over ES2. These Mg^{2+}-induced changes in the populations of ES1 and ES2 explain the Mg^{2+}-induced changes in line-broadening observed in 2D ^1H,^{13}C-HSQC spectra (Supplementary Figure S2).

Characterizing ES structures

The aromatic C6/C8 chemical shifts ($\Delta\omega$) provide fingerprints that can be used to assess structural features of the ES (79). In general, nucleotides that adopt a stacked *anti* conformation fall within a specific region of the spectrum along with Watson–Crick base pair. Relative to this 'helical' reference, unpaired bulged out nucleotides or *syn* nucleotide bases tend to have downfield shifted ($\Delta\omega > 2$ ppm) aromatic C6/C8 chemical shifts. For a system in fast exchange on the NMR timescale and in equilibrium between the two states, the extent of the downfield shift could be moderated by the relative populations of the different species. Such structural inferences made from analysis of chemical shifts have to be tested independently, typically with the use of mutations to change the exchange dynamics.

We analyzed the RREIIB ES1 and ES2 chemical shifts to gain insight into their conformations (Supplementary Table S1) (16–18). Many nucleotides (U72-C6, G71-C8 and G46-C8) had similar chemical shift fingerprints indicating that they adopt similar conformations in ES1 and ES2. For example, U72-C6, $\Delta\omega_{ES1} = -2.3$ ppm and $\Delta\omega_{ES2} = -1.2$ ppm suggest a bias toward a helical conformation; G71-C8 was significantly upfield shifted ($\Delta\omega_{ES1} = -3.8$ ppm and $\Delta\omega_{ES2} = -1.6$ ppm) suggesting a more helical *anti* conformation; while for G46-C8, $\Delta\omega_{ES1} = 1.1$ ppm and $\Delta\omega_{ES2} = 1.1$ ppm suggest a less helical conformation (Supplementary Table S1). The fingerprints for G71-C8 and U72-C6 (larger $\Delta\omega$,

see Supplementary Table S1) suggest a more helical conformation in ES1 as compared to the GS or ES2 (79).

Other nucleotides have different chemical shift fingerprints indicating that they adopt different conformations in ES1 and ES2. For example, G47-C8 in ES1 ($\Delta\omega_{ES1} = 4.0$ ppm) suggests a *syn* base conformation, but a mixture of *syn* and *anti* conformations in ES2 with a moderate downfield shift ($\Delta\omega_{ES2} = 1.6$ ppm) (Supplementary Table S1). A68-C8 did not show any exchange due to ES1, and $\Delta\omega_{ES2} = -2.5$ ppm suggests a more helical conformation in ES2. No residues showed exchange due to ES1 but not ES2 (Supplementary Table S1), and ES1 and ES2 conformations are further verified in the following sections.

MC-fold (81) was used to predict alternative low energy secondary structures for RREIIB. Strikingly, the two lowest energy structures following the GS could explain the ES1 and ES2 chemical shift fingerprints (Supplementary Figure S3D). The putative ES1 structure forms by migrating the lower U72 bulge upwards by having U72 displace G71 for pairing with G48, while G71 displaces G70 for pairing with C49, leaving G70 bulged out (Figure 3A). This putative ES1 structure also features a G48-U72 mismatch and C49-G71 base pair, which can explain the increase in helical character relative to the GS at U72 and G71, respectively, while A68 remains bulged out, explaining lack of ES1 RD at this site. The putative ES1 structure also features a G47-A73 mismatch. If this mismatch was to adopt a Hoogsteen type G(*syn*)-A$^+$(*anti*) conformation, the *syn* base could explain the large downfield-shift at G47-C8 in ES1.

To obtain additional evidence for protonation of A73 in ES1, we carried out pH-dependent 2D ^1H,^{13}C-HSQC measurements on RREIIB and observed the expected upfield shift for A73-C8 at higher pH consistent with perturbing equilibrium toward GS (Supplementary Figure S4A). In contrast, lowering the pH resulted in further line-broadening such that even A73-C8H8 was no longer observable, consistent with an increase in the population of protonated ES1 (Supplementary Figure S4A). Finally, we also carried out RD measurements on G47-C8 that reports on ES1 at higher pH = 8 and observed the expected decrease
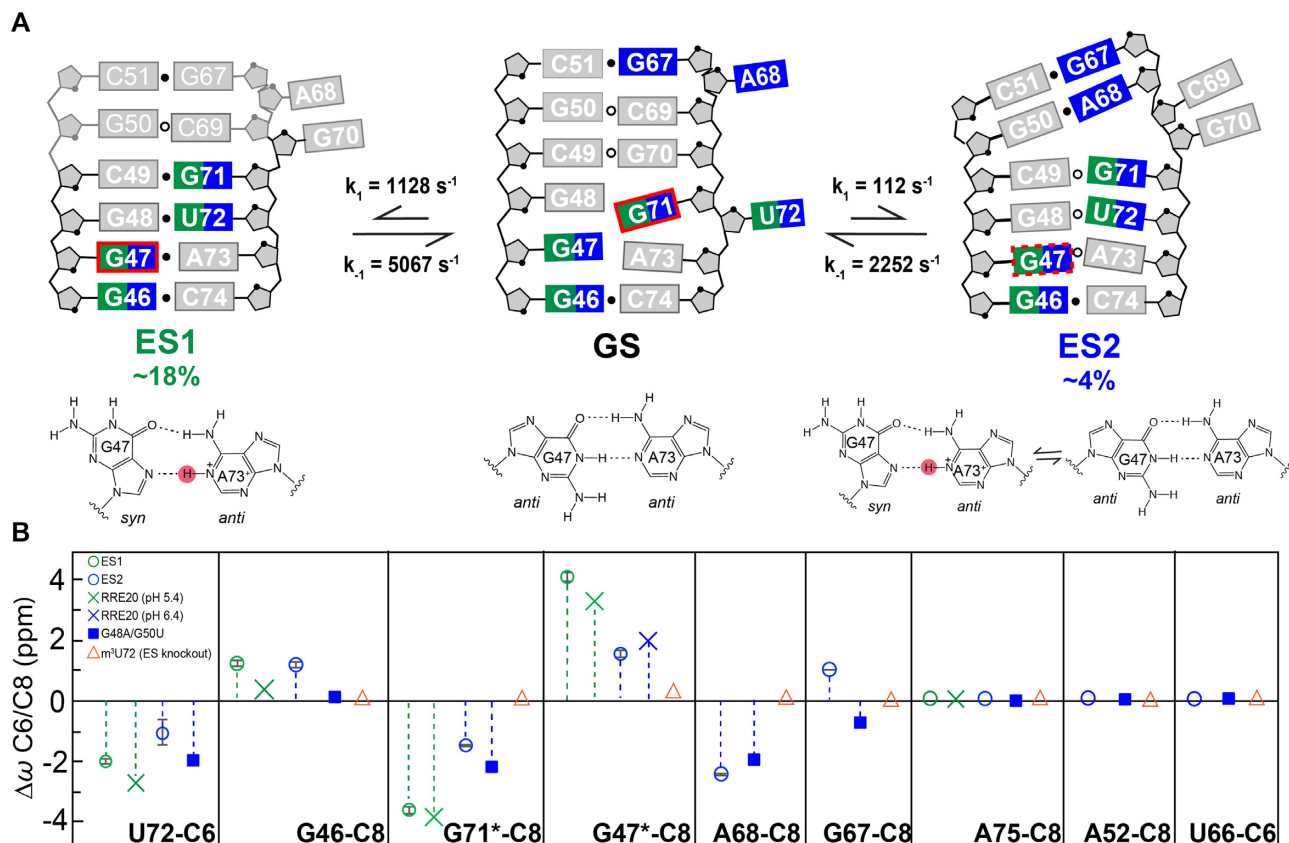
Figure 3. Chemical shift fingerprinting RRE ESs. (**A**) Putative secondary structure of RREIIB ES1 and ES2. Nucleotides that experience exchange due to ES1 and ES2 are colored green and blue, respectively. *Syn* bases are indicated with red boxes. The G47(*syn*)–A73$^+$(*anti*) $\rightleftharpoons$ G47(*anti*)–A73(*anti*) equilibrium indicated with the red-dashed box on ES2. The different G47–A73 conformations in GS, ES1 and ES2 are shown below the secondary structures. Base pairs with and without detectable H-bonds are indicated using filled and empty circles, respectively. (**B**) Comparison of $\Delta\omega = \omega_{ES} - \omega_{GS}$ obtained using RD (values obtained in the absence of Mg^{2+} indicated using asterisk) with corresponding $\Delta\omega_{mut} = \omega_{ES\text{-}mutant} - \omega_{wild\text{-}type}$ obtained for the mutants. Buffer conditions: 15 mM sodium phosphate, 25 mM NaCl, 0.1 mM EDTA, pH 6.4 with or without 3 mM MgCl$_2$.

in RD consistent with destabilization of ES1 (population < 0.01%, Supplementary Figure S4B).

On the other hand, the putative ES2 structure forms by downward migration of the upper stem IIB bulge. Here, A68 displaces C69 for pairing with G50, and this is accompanied by the additional flipping out of G70 possibly to accommodate the junctional G50-A68 (Figure 3A). This putative ES2 structure can explain the increase in helical character relative to the GS observed at A68 that likely forms G50(*anti*)–A68(*anti*) mismatch based on the chemical shifts. The putative ES2 structure also features a G47-A73 mismatch, which based on the weakly downfield shifted G47-C8 ($\Delta\omega_{ES2}$ = 1.6 ppm) that is predicted to form a ~50:50 G47(*anti*)–A73(*anti*) $\rightleftharpoons$ G47(*syn*)–A73$^+$(*anti*) dynamic equilibrium. In contrast, to G47-C8, increasing the pH to 8 had a negligible effect on ES2 exchange as judged based on RD measurements on A68-C8 (population changed from ~11% to ~10%, Supplementary Figure S4B and C). This is consistent with the absence of a predominantly protonated mismatch in ES2.

It should be noted that among the predicted secondary structures are close variants of the proposed ES1 and ES2 that feature small variations with respect to which nucleotides are junctional versus unpaired (ES1* and ES2* in

Supplementary Figure S3D). We cannot rule out that such conformations also exist in 10-fold lower abundance relative to the ESs characterized here.

Testing non-native ES structures using mutate-and-chemical shift fingerprinting

A mutate-and-chemical-shift-fingerprinting strategy (16) was used to test the proposed ES structures (Figure 3 and Supplementary Figure S5). Mutations were introduced to stabilize conformational features unique to the two ESs. The chemical shifts of the mutant relative to wild-type ($\Delta\omega_{mut}$) were then compared to those measured by RD ($\Delta\omega_{RD}$).

ES1 and ES2 share a similar lower helical stem with G47-A73 and G48-U72 mismatches. This stem was stabilized using a hairpin construct (UUCG-RRE20) capped by a stable UUCG loop (Supplementary Figure S5A). NMR analysis revealed that UUCG-RRE20 folds into the expected secondary structure (Supplementary Figure S6). Very good agreement was observed between $\Delta\omega_{mut}$ and $\Delta\omega_{RD}$ measured for ES1 and ES2 for U72-C6, G46-C8 and G71-C8 (Figure 3B and Supplementary Figure S5B). In addition, sites that showed no detectable RD (A75-C8, A52-C8, U66-

C6 and G53-C8) also experienced very small chemical shift perturbations (Figure 3B and Supplementary Figure S5B).

ES1 and ES2 differ significantly with regards to the chemical shift fingerprints for G47-C8. At pH 6.4, G47-C8 in UUCG-RRE20 was only partially downfield shifted ($\Delta\omega_{mut}$ = 1.7 ppm) in very good agreement with the ES2 chemical shifts ($\Delta\omega_{RD}$ = 1.6 ppm). A strong H8-H1′ NOE cross peak was also observed (Supplementary Figure S6) indicating that G47 at least partially adopts the predicted *syn* conformation consistent with the proposed ∼50:50 G47(*anti*)–A73(*anti*) ⇌ G47(*syn*)–A73$^+$(*anti*) equilibrium. This is notable considering that G-A mismatches can adopt a wide range of pairing geometries (G(*syn*)–A$^+$(*anti*), G(*anti*)–A(*syn*) and G(*anti*)–A(*anti*)) depending on sequence, structural context and pH (82–85). Lowering the pH to 5.4 resulted in the expected fully downfield shifted G47-C8 (3.3 ppm) in good agreement with the RD derived ES1 chemical shifts ($\Delta\omega_{RD}$ = 4 ppm) (Figure 3B and Supplementary Figure S6). Protonation of A73 would also help explain why the A73-C2H2 resonance is broadened out of detection given that protonation is accompanied by a large (∼6 ppm) shift in adenine-C2 and also the downfield shift observed for A73-C8 (86) (Supplementary Figure S6). Lowering the pH had little effect on other resonances, indicating that in the mutant RRE20 (but not necessarily the ES), the G47(*anti*)–A73(*anti*) ⇌ G47(*syn*)–A73$^+$(*anti*) equilibrium is decoupled from any other conformational changes in the molecule (Supplementary Figure S6).

A second mutant (UUCG-G48A/G50U) was designed to stabilize the non-canonical G48-U72 and G50-A68 mismatches in ES2 (Supplementary Figure S5A). NMR analysis indicates that UUCG-G48A/G50U folds into the putative ES2 secondary structure with G48-U72 and G50(*anti*)–A68(*anti*) mismatches and a dinucleotide C69-G70 bulge (Supplementary Figure S7). This provided independent support for proposed dinucleotide bulge in ES2 for which no RD data could be measured. Again, excellent agreement was observed between $\Delta\omega_{mut}$ and $\Delta\omega_{RD}$ for U72-C6, G46-C8, G71-C8 and A68-C8 (Figure 3B and Supplementary Figure S5B). The only exception was G47-C8 for which the chemical shifts and NOEs indicate that the G47-A73 adopts an *anti–anti* conformation with chemical shifts similar to the GS. Thus, the UUCG-G48A/G50U mutant does not appear to capture G47-A73 in the ES2. This is not surprising considering that the neighboring residue is mutated and *syn*:*anti* equilibria are known to be quite dependent on sequence context (87).

Finally, we also tested a mutant designed to destabilize both ES1 and ES2 through introduction of the chemically modified m³U72 (m³U72-RREIIB) that blocks formation of the G48-U72 mismatch in ES1 and ES2 without affecting the GS in which U72 is bulged out (Supplementary Figure S8A). As expected, 2D NMR spectra of m³U72-RREIIB were mostly identical their unmodified counterparts, with minor differences observed in and around the site of modification (Figure 3B and Supplementary Figure S5B). Interestingly, some resonances such as G47 and G71 shifted toward the GS (Supplementary Figure S8A). The modification also reduced line broadening in 2D NMR spectra at G48, G71 and A73 exactly as expected from destabilization of both ES1 and ES2 (Supplementary Figure S8B). This

provides independent support that U72 is paired in ES1 and ES2.

Characterizing ESs in the RREII three-way junction

Examining whether or not the ESs also form in the large RREII construct (68 nt) is complicated by severe spectral overlap and low sensitivity in this larger RNA particularly when resonances are broadened due to conformational exchange. Recognizing that the ES1 population in RREIIB is quite high (p_B ∼18%), we reasoned that it may be possible to directly observe ES1 in RREII provided that specific sites (^{15}N3-U72, ^{13}C6-U72 or ^{13}C8-G71) were labeled to aid observation of resonances belonging to the minor ES populations from the overwhelming excess of resonances belonging to the dominant GS. If exchange in RREII was slow on the NMR timescale, it should be feasible to directly observe the chemical shifts of ES1 and thereby also estimate its population (Figure 4). If on the other hand, exchange was fast on the NMR timescale, as is observed in RREIIB ($\Delta\omega/k_{ex}$ = 2.4), the population weighted chemical shifts for nucleotides that experience large $\Delta\omega$ would be shifted toward either GS or ES, in a manner dependent on their relative populations. The strategy therefore affords the possibility to detect ESs in large RNAs under both fast and slow exchange conditions.

The U72 imino resonance is not observable in the GS, because it adopts an unpaired conformation (Figure 4A). In contrast, not only should this resonance be observable in both ES1 and ES2, but predicted to resonate at specific NMR chemical shifts unique to the G-U wobble (Figure 4A). We recorded NMR spectra for ^{15}N3-U72-RREII in the presence of 3 mM Mg^{2+}. Under these conditions and based on RD measured in RREIIB, we expect ES1 p_B ∼18% and ES2 p_B ∼ 4%. Strikingly, NMR spectra of ^{15}N3-U72-RREII revealed a single uridine imino resonance with ^{1}H and ^{15}N chemical shifts that are characteristic of a G-U wobble (Figure 4B). To further confirm direct observation of ES1 in RREII, we selectively labeled ^{13}C6-U72 and observed a major resonance corresponding to the GS, in which U72 is bulged out, and a minor upfield-shifted resonance (-2.7 ppm) that is in excellent agreement with the chemical shift measured for ES1 using RD ($\Delta\omega_{RD}$ = −2.3 ± 0.1 ppm) and in poorer agreement with ES2 ($\Delta\omega_{RD}$ = 1.2 ± 0.5 ppm) (Figure 4C). Finally, we also prepared a sample with labeled ^{13}C8-G71 and observed the expected major resonance corresponding to the GS in which G71 forms G48-G71(*syn*) and a minor upfield-shifted (−4.1 ppm) resonance that presents an *anti*-base of G71 in excellent agreement with ES1 chemical shift ($\Delta\omega_{RD}$ = −3.8 ± 0.2 ppm) and poorer agreement with ES2 ($\Delta\omega_{RD}$ = −1.6 ± 0.05 ppm) (Figure 4C). These spectra were recorded in the absence of Mg^{2+} to allow comparison with RD data on RREIIB and under these conditions we expect ES1 p_B ∼ 6% and ES2 p_B ∼ 11%.

The population of ES1 estimated from the integrated volumes of the resonances is ∼20% in the absence or presence of 3 mM Mg^{2+}. This is in good agreement with ES1 population (∼18%) measured in RREIIB in the presence of 3 mM Mg^{2+}. Taken together, these data show that ES1 also exists in RREII three-way junction with similar populations
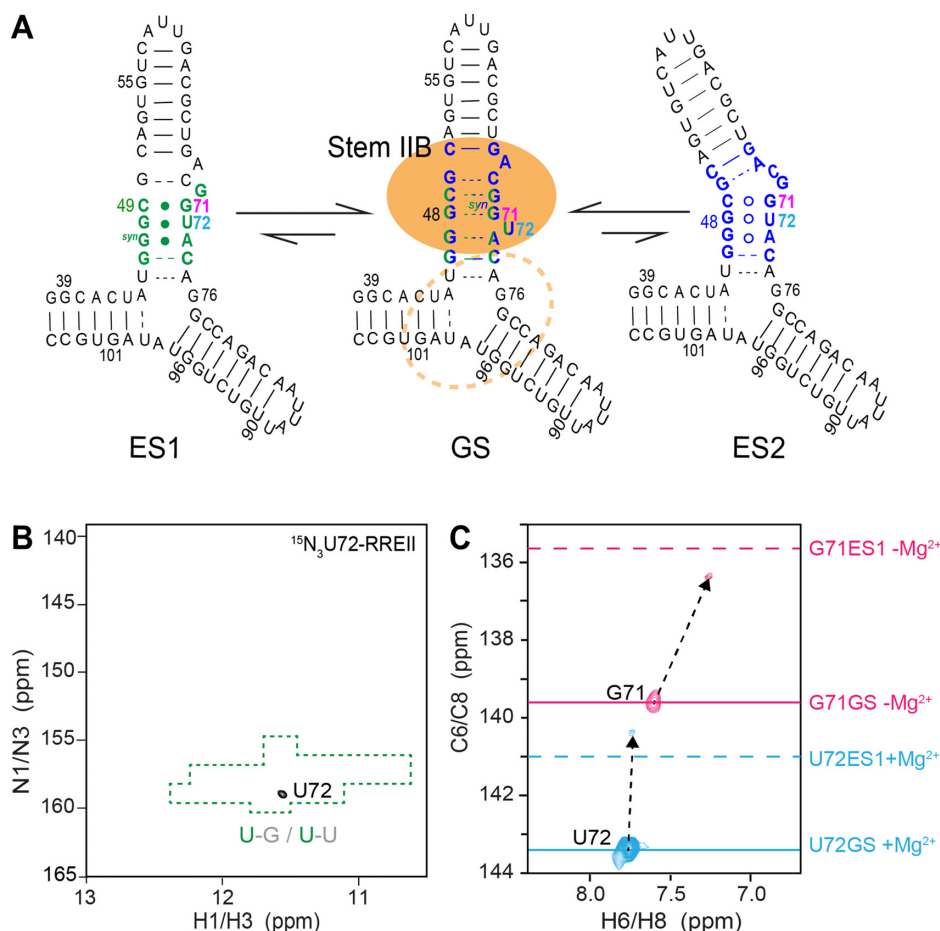
Figure 4. Selective labeling strategy to probe conformational exchange in RREII. (**A**) Proposed secondary structure for ES1 and ES2 in RREII based on ESs observed in RREIIB. Nucleotides that experience exchange due to ES1 and ES2 are colored green and blue, respectively. Rev primary and secondary binding sites are highlighted using a filled and dashed orange circle, respectively. (**B**) 2D ^{1}H,^{15}N-HSQC spectrum of site-specifically labeled ^{15}N3-U72-RREII at 25°C in 3 mM Mg^{2+} showing a single imino resonance at the characteristic chemical shift region (highlighted in green) expected for a G-U wobble. (**C**) 2D ^{1}H,^{13}C-HSQC spectra of site-specifically labeled ^{13}C6-U72-RREII (pink) and ^{13}C8-G71-RREII (cyan) at 25°C showing the appearance of major resonances consistent with the GS in RREIIB (solid line) and minor resonances consistent with ES1 in RREIIB (dashed line). Spectra for ^{13}C8-G71-RREII were measured in the absence of Mg^{2+}. The sample conditions were 0.2–0.3 mM RREII in 15 mM sodium phosphate, 25 mM NaCl, 0.1 mM EDTA, pH 6.4 with or without 3 mM MgCl$_2$.

as RREIIB and that the three-way junction decouples the dependence of the ES1 population on Mg^{2+}. While we do not observe ES2 resonances, we cannot rule out that the exchange is too fast or that the ES2 population falls below detection limit in this experiment. Indeed, these ES2 resonances were also not observed in corresponding site-labeled RREIIB samples likely due to fast-exchange. This suggests that the ES2 population in RREII is too low and/or lifetime too short for direct detection using this approach. These results establish site-specific labeling as a new methodology for directly observing ESs in large RNAs.

Rev peptide binds the RRE ESs with significantly lower affinity

The ES1 and ES2 conformations disrupt structural elements in stem IIB that have previously been shown to be critical for Rev binding. The hypothesis that Rev-ARM peptide binds more weakly to the non-native ES1 and ES2 was tested using a mutate-and-rescue strategy. The Rev-ARM–stem IIB interaction has been shown to recapitulate the affinity and specificity of the full complex (48,88). We tested the impact of mutations that stabilize ES1 and/or ES2 on binding of fluorescein-labeled Rev-ARM peptide (Rev-Fl) using a fluorescence polarization (FP) assay (78). The ES-stabilizing mutants used in NMR chemical shift fingerprinting eliminate structural elements required for Rev binding and also do not afford the possibility to introduce rescue mutations. We therefore designed a new set of ES-stabilizing mutants that preserve key elements required for Rev binding and that could be rescued with compensatory mutations (Figure 5A). This was not a simple task given the need to avoid mutating residues important for Rev recognition.

ES2 was stabilized using the A68C point substitution mutation, which replaces the non-canonical G50-A68 mismatch with a canonical G50-C68 Watson–Crick base pair. Both ES1 and ES2 were stabilized using the U72C point substitution mutation, which replaces the G48-U72 wobble with a canonical G48-C72 Watson–Crick base pair (Figure
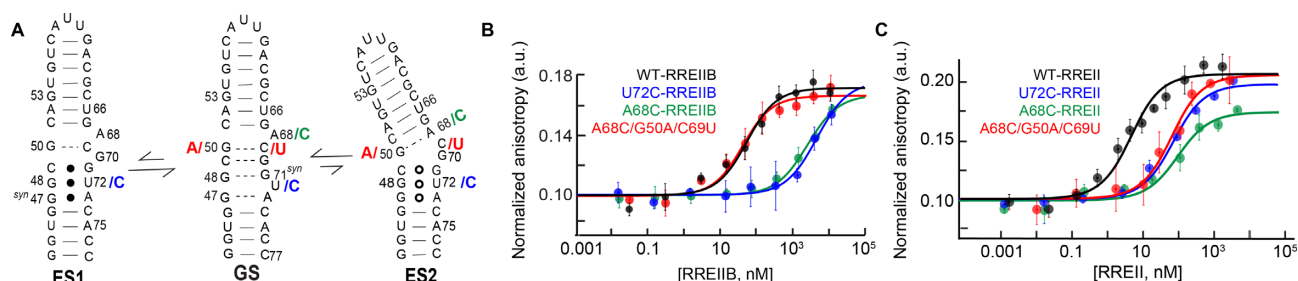
Figure 5. Measurement of the binding affinity between Rev-ARM peptide and RRE, ES-stabilizing mutants and rescue mutants using fluorescence polarization. (**A**) The designed ES-stabilizing, ES2-stabilizing and ES2-rescue mutants are colored in blue, green and red, respectively. (**B-C**) Normalized anisotropy values measured for RREIIB (**B**)and RREII (**C**) fitted with one-site binding model (see 'Materials and Methods' section). The anisotropy value observed in the absence of RNA was normalized to 0.1. Uncertainty reflects the standard deviation from three independent measurements. Buffer conditions: 30 mM HEPES, pH = 7.0, 100 mM KCl, 10mM sodium phosphate, 10 mM ammonium acetate, 10 mM guanidinium chloride, 2 mM $MgCl_2$, 20 mM NaCl, 0.5 mM EDTA and 0.001% (v/v) Triton-X100. Concentration of Rev-Fl peptide was 10 and 1 nM for RREIIB and RREII respectively.

5A). While these mutations were predicted to fold into the ESs as the energetically preferred conformation, the NMR spectra show significant line-broadening specifically at nucleotides (U72 and A68) involved in the conformational exchange (Supplementary Figure S9A and B). These data indicate that the mutants push the conformational equilibrium toward the ESs (to ∼50% population) but to a smaller degree than the more stringent mutations used in mutate-and-chemical-shift-fingerprinting (Figure 3). We also cannot rule out that the mutations populate other higher energy ESs (Supplementary Figure S3D) that may contribute to the observed line-broadening.

As a positive control, Rev-Fl peptide binds to wild-type RREIIB with $K_d = 45.9 \pm 15.2$ nM (Figure 5B and Table 1) in good agreement with prior studies (∼30–50 nM) (48,88). The binding affinity ($K_d > 2000$ nM) decreased 40- to 80-fold for the A68C and U72C RREIIB mutants (Table 1). Because of the reduced binding affinity, binding did not reach saturation, and increasing the concentration of the ES-stabilized mutants further resulted in additional low-affinity binding (89) (Supplementary Figure S10A). To test whether the reduction in binding affinity is due to stabilization of the unique ES conformation, we introduced additional rescue mutations (A68C/G50A/C69U-RREIIB and Figure 5A) designed to restore the GS conformation by stabilizing an A50-U69 canonical base pair in the mutant. Indeed, the rescue mutant restored Rev binding to wild-type levels ($K_d = 33.0 \pm 11.3$ nM) (Figure 5B and Table 1). Thus, the lower binding affinity observed for the ES-stabilizing mutants is due to their alternative conformations and not due to changes in sequence.

The ES-stabilizing mutations also weakened binding to the three-way junction RREII (Figure 5C). As a positive control, Rev-Fl binds to wild-type RREII with 30-fold higher affinity ($K_d = 1.5 \pm 0.4$ nM) compared to RREIIB, consistent with prior studies that report affinities on the order of ∼3–9 nM (Table 1) (48,78). Binding to the A68C and U72C RREII ES stabilizing mutants was reduced ∼15 fold ($K_d > 20$ nM, Table 1). Once again, because of the low binding affinity, the binding curves did not reach saturation and further addition of ES-stabilizing mutants resulted in additional low-affinity binding (Supplementary Figure S10A). In RREII, the A68C ES2 rescue mutant (A68C/G50A/C69U-RREII) only partially restored wild-

Table 1. The apparent K_d describing binding of wild-type RREIIB and RREII and their mutants to Rev-Fl obtained by fitting binding curves to a one-site binding model

	Apparent K_d (nM)
RREIIB	
WT	45.9 ± 15.2
A68C	>2000
U72C	>4000
A68C/G50A/C69U	33.0 ± 11.3
m^3U72	36.2 ± 9.3
RREII	
WT	1.5 ± 0.4
A68C	>25
U72C	>22
A68C/G50A/C69U	15.4 ± 5.1

Uncertainty represents standard deviation over triplicate measurements. The concentration of Rev-Fl peptide is 10 and 1 nM for RREIIB and RREII, respectively. Buffer conditions: 30 mM HEPES, pH = 7.0, 100 mM KCl, 10 mM sodium phosphate, 10 mM ammonium acetate, 10 mM guanidinium chloride, 2 mM $MgCl_2$, 20 mM NaCl, 0.5 mM EDTA and 0.001% (v/v) Triton-X100

type binding ($K_d = 15.5 \pm 5.1$ nM). The binding affinity measured for the rescue mutant was more similar to that observed for the same rescue mutant in RREIIB ($K_d = 33.0 \pm 11.3$ nM) as compared to the wild-type sequences where the differences were 30-fold. This indicates that the higher affinity to RREII relative to RREIIB may be linked to nucleotides G50 and C69 used in the rescue mutations.

Finally, we measured the binding to ES-destabilizing mutant m^3U72-RREIIB. Increasing the binding-competent GS from 80% to 100% is predicted to improve the binding and decrease the observed K_d. Indeed, as expected, the binding affinity ($K_d = 36.2 \pm 9.3$ nM, Supplementary Figure S10B and Table 1) did slightly increase in the ES knock-out mutant.

DISCUSSION

Our study adds to a growing view that non-canonical regions of RNA do not fold into a single secondary structure but rather exist as a dynamic equilibrium of alternative conformations that have non-native secondary structure (16–19). Relative to other RNA ESs, which tend to have populations on the order of ∼1%, the ES population in RREII
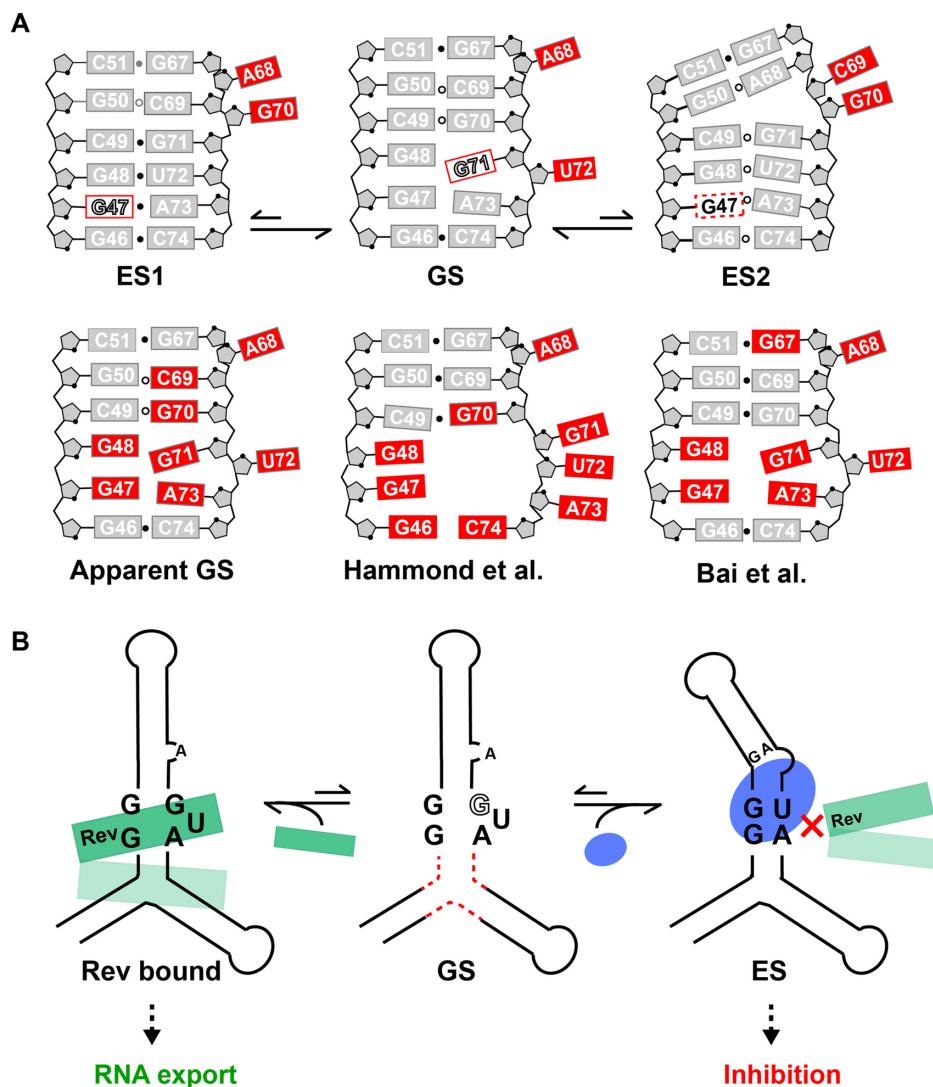
Figure 6. Implications of RRE dynamic ensemble. (**A**) The RRE ES ensemble results in different conformations that expose different nucleotides for reactivity. This could contribute to high reactivity (apparent GS) at several nucleotides (colored in red), including ones that may form canonical pairs in the GS. Results are compared with SHAPE reactivity measured previously by Hammond *et al.* (90) and Bai *et al.* (42). The *syn* base in GS and ES1 are indicated using red rectangles and open letters. Residues in *syn* to *anti* conformational exchange are indicated using dashed rectangles. (**B**) Proposed role for RRE ESs in providing mechanisms for conformational cooperativity during Rev (in green) recognition by organizing the secondary binding site (dashed red lines). Stabilization of ESs using small molecules (in blue) could provide a strategy for inhibiting Rev binding and viral RNA export for *anti*-HIV therapeutics. The *syn* base is indicated using open letters.

is ∼20% in the presence of Mg²⁺. Given that the RRE ESs bind Rev peptides with 15- to 80-fold weaker affinity, these results underscore how subtle reshuffling of base pairs can lead to RNA conformations with very different biological activities.

The high population of the ESs also implies that they could contribute to chemical probing data, which is averaged over the ensemble. In this regard, the RRE ensemble helps clarify the high SHAPE reactivity reported in previous studies for many nucleotides within the internal loop of stem IIB, which are base paired in the GS (42,90). For example, in ES1, G70 flips out and G47 adopts a non-canonical *syn* conformation, and this could explain the high reactivity at these nucleotides (Figure 6A) (42,90). Importantly, while the ES ensemble predicts that many nucleotides will be un-

paired at a given point in time, they are seldom unpaired simultaneously. This emphasizes the importance of interpreting chemical probing data in terms of dynamic ensembles (30,31). Ensemble-based approaches (29,30,91) for interpreting chemical probing data may help clarify the nature of the stem II RRE ensemble within the complex cellular environment. Indeed, the ensemble cannot explain the high SHAPE reactivity at G46-C74 (90), which is paired in all conformations. Thus, we cannot rule out that the RRE ensemble differs in the complex cellular environment as compared to *in vitro*.

The addition of the three-way junction did induce small perturbations at stem IIB (Supplementary Figure S9A and B). In addition, mutations to stem IIB that stabilize the ES-induced changes in chemical shifts outside stem IIB in the

RREII three-way junction (Supplementary Figure S9C). Thus, it is possible that formation of the ESs in stem IIB is correlated with other conformational changes at the three-way junction region. Because of this conformational coupling, binding of Rev to stem IIB could help organize the second binding site at the three-way junction, including possibly by diminishing the population of any ESs, and thereby provide an additional source of binding cooperativity based on RNA conformational dynamics. Indeed, prior studies showed that replacement of the three-way junction with a stable duplex leads to loss of binding cooperativity (48). Further studies are needed to test this hypothesis. In this regard, the new site-specific labeling strategy introduced in this work provides a new means by which to extend our studies and examine ESs in the RRE stem II three-way junction.

The RRE ensemble also helps with the interpretation of the extensive mutagenesis studies done on the RRE stem IIB (58,60,92,93). These mutations have been shown to inhibit Rev binding by 60- to 2000-fold (58,60,92,93) and to suppress activity in cell based assays by up to 90% (58,60). Interestingly, none of these prior mutations are predicted to stabilize ES1 or ES2. Rather, they are predicted to disrupt key nucleotides (G47, G48, C49, G70, G71, A73) required for Rev binding. Thus, the reduced binding affinity or activity observed with these prior mutations most likely reflects changes in the contacts and/or conformation of the RRE GS, and not stabilization of alternative ESs.

The RRE stem IIB has been the subject of much effort directed toward the development of small molecule *anti*-HIV therapeutics (36–38,40). Most of these studies have relied on high-throughput screening and/or the rational design of inhibitors that target the RRE GS (36–38,40). The new non-native ESs, which remodel key structural features required for Rev binding could constitute novel states for targeting with small molecules (Figure 6B). Determining the structures of the RRE ESs would make it possible to apply ensemble-based virtual screening approaches (12,13) to identify small molecule that selectively bind the ESs. The ES-stabilizing mutants could also be subjected to high-throughput screening to help identify compounds that selectively bind these non-native states. Because of their unique allosteric mode of action, the hits emerging from such studies might offer complimentary path toward development of *anti*-HIV therapeutics relative to approaches targeting the dominant GS.

SUPPLEMENTARY DATA

Supplementary Data are available at NAR Online.

ACKNOWLEDGEMENTS

FUNDING

REFERENCES

1. Cech,T.R. and Steitz,J.A. (2014) The noncoding RNA revolution-trashing old rules to forge new ones. *Cell*, **157**, 77–94.
2. Chen,Y.G., Satpathy,A.T. and Chang,H.Y. (2017) Gene regulation in the immune system by long noncoding RNAs. *Nat. Immunol.*, **18**, 962–972.
3. He,L. and Hannon,G.J. (2004) MicroRNAs: small RNAs with a big role in gene regulation. *Nat. Rev. Genet.*, **5**, 522–531.
4. Childs-Disney,J.L. and Disney,M.D. (2016) Approaches to validate and manipulate RNA targets with small molecules in cells. *Annu. Rev. Pharmacol. Toxicol.*, **56**, 123–140.
5. Howe,J.A., Wang,H., Fischmann,T.O., Balibar,C.J., Xiao,L., Galgoci,A.M., Malinverni,J.C., Mayhood,T., Villafania,A., Nahvi,A. *et al.* (2015) Selective small-molecule inhibition of an RNA structural element. *Nature*, **526**, 672–677.
6. Connelly,C.M., Moon,M.H. and Schneekloth,J.S. Jr. (2016) The emerging role of RNA as a therapeutic target for small molecules. *Cell Chem. Biol.*, **23**, 1077–1090.
7. McKeague,M., Wong,R.S. and Smolke,C.D. (2016) Opportunities in the design and application of RNA for gene expression control. *Nucleic Acids Res.*, **44**, 2987–2999.
8. Qi,L.S. and Arkin,A.P. (2014) A versatile framework for microbial engineering using synthetic non-coding RNAs. *Nat. Rev. Microbiol.*, **12**, 341–354.
9. Dethoff,E.A., Chugh,J., Mustoe,A.M. and Al-Hashimi,H.M. (2012) Functional complexity and regulation through RNA dynamics. *Nature*, **482**, 322–330.
10. Cruz,J.A. and Westhof,E. (2009) The dynamic landscapes of RNA architecture. *Cell*, **136**, 604–609.
11. Furtig,B., Nozinovic,S., Reining,A. and Schwalbe,H. (2015) Multiple conformational states of riboswitches fine-tune gene regulation. *Curr. Opin. Struct. Biol.*, **30**, 112–124.
12. Stelzer,A.C., Frank,A.T., Kratz,J.D., Swanson,M.D., Gonzalez-Hernandez,M.J., Lee,J., Andricioaei,I., Markovitz,D.M. and Al-Hashimi,H.M. (2011) Discovery of selective bioactive small molecules by targeting an RNA dynamic ensemble. *Nat. Chem. Biol.*, **7**, 553–559.
13. Ganser,L.R., Lee,J., Rangadurai,A., Merriman,D.K., Kelly,M.L., Kansal,A.D., Sathyamoorthy,B. and Al-Hashimi,H.M. (2018) High-performance virtual screening by targeting a high-resolution RNA dynamic ensemble. *Nat. Struct. Mol. Biol.*, **25**, 425–434.
14. Frauenfelder,H., Sligar,S.G. and Wolynes,P.G. (1991) The energy landscapes and motions of proteins. *Science*, **254**, 1598–1603.
15. Mustoe,A.M., Brooks,C.L. and Al-Hashimi,H.M. (2014) Hierarchy of RNA functional dynamics. *Annu. Rev. Biochem.*, **83**, 441–466.
16. Dethoff,E.A., Petzold,K., Chugh,J., Casiano-Negroni,A. and Al-Hashimi,H.M. (2012) Visualizing transient low-populated structures of RNA. *Nature*, **491**, 724–728.
17. Lee,J., Dethoff,E.A. and Al-Hashimi,H.M. (2014) Invisible RNA state dynamically couples distant motifs. *PNAS*, **111**, 9485–9490.
18. Xue,Y., Gracia,B., Herschlag,D., Russell,R. and Al-Hashimi,H.M. (2016) Visualizing the formation of an RNA folding intermediate through a fast highly modular secondary structure switch. *Nat. Commun.*, **7**, doi:10.1038/ncomms11768.
19. Zhao,B., Guffy,S.L., Williams,B. and Zhang,Q. (2017) An excited state underlies gene regulation of a transcriptional riboswitch. *Nat. Chem. Biol.*, **13**, 968–974.
20. Denny,S.K., Bisaria,N., Yesselman,J.D., Das,R., Herschlag,D. and Greenleaf,W.J. (2018) High-Throughput investigation of diverse junction elements in RNA tertiary folding. *Cell*, **174**, 377–390.
21. Korzhnev,D.M., Orekhov,V.Y. and Kay,L.E. (2005) Off-resonance R(1rho) NMR studies of exchange dynamics in proteins with low spin-lock fields: an application to a Fyn SH3 domain. *J. Am. Chem. Soc.*, **127**, 713–721.
22. Zhou,H., Kimsey,I.J., Nikolova,E.N., Sathyamoorthy,B., Grazioli,G., McSally,J., Bai,T., Wunderlich,C.H., Kreutz,C., Andricioaei,I. *et al.*

(2016) m(1)A and m(1)G disrupt A-RNA structure through the intrinsic instability of Hoogsteen base pairs. *Nat. Struct. Mol. Biol.*, **23**, 803–810.

23. Kimsey,I.J., Szymanski,E.S., Zahurancik,W.J., Shakya,A., Xue,Y., Chu,C.C., Sathyamoorthy,B., Suo,Z.C. and Al-Hashimi,H.M. (2018) Dynamic basis for dG.dT misincorporation via tautomerization and ionization. *Nature*, **554**, 195–201.

24. Sun,X., Zhang,Q. and Al-Hashimi,H.M. (2007) Resolving fast and slow motions in the internal loop containing stem-loop 1 of HIV-1 that are modulated by Mg2+ binding: role in the kissing-duplex structural transition. *Nucleic Acids Res.*, **35**, 1698–1713.

25. Gracia,B., Al-Hashimi,H.M., Bisaria,N., Das,R., Herschlag,D. and Russell,R. (2018) Hidden structural modules in a cooperative RNA folding transition. *Cell Rep.*, **22**, 3240–3250.

26. Zhao,B. and Zhang,Q. (2015) Characterizing excited conformational states of RNA by NMR spectroscopy. *Curr. Opin. Struct. Biol.*, **30**, 134–146.

27. Kloiber,K., Spitzer,R., Tollinger,M., Konrat,R. and Kreutz,C. (2011) Probing RNA dynamics via longitudinal exchange and CPMG relaxation dispersion NMR spectroscopy using a sensitive 13C-methyl label. *Nucleic Acids Res.*, **39**, 4340–4351.

28. Steiner,E., Schlagnitweit,J., Lundstrom,P. and Petzold,K. (2016) Capturing excited states in the Fast-Intermediate exchange limit in biological systems using (1) H NMR spectroscopy. *Angew. Chem. Int. Ed. Engl.*, **55**, 15869–15872.

29. Tian,S., Cordero,P., Kladwang,W. and Das,R. (2014) High-throughput mutate-map-rescue evaluates SHAPE-directed RNA structure and uncovers excited states. *RNA*, **20**, 1815–1826.

30. Spasic,A., Assmann,S.M., Bevilacqua,P.C. and Mathews,D.H. (2018) Modeling RNA secondary structure folding ensembles using SHAPE mapping data. *Nucleic Acids Res.*, **46**, 314–323.

31. Li,H. and Aviran,S. (2018) Statistical modeling of RNA structure profiling experiments enables parsimonious reconstruction of structure landscapes. *Nat. Commun.*, **9**, 606.

32. Malim,M.H., Hauber,J., Le,S.Y., Maizel,J.V. and Cullen,B.R. (1989) The HIV-1 rev trans-activator acts through a structured target sequence to activate nuclear export of unspliced viral mRNA. *Nature*, **338**, 254–257.

33. Chang,D.D. and Sharp,P.A. (1989) Regulation by HIV Rev depends upon recognition of splice sites. *Cell*, **59**, 789–795.

34. Malim,M.H., Tiley,L.S., McCarn,D.F., Rusche,J.R., Hauber,J. and Cullen,B.R. (1990) HIV-1 structural gene expression requires binding of the Rev trans-activator to its RNA target sequence. *Cell*, **60**, 675–683.

35. Malim,M.H. and Cullen,B.R. (1991) HIV-1 structural gene expression requires the binding of multiple Rev monomers to the viral RRE: implications for HIV-1 latency. *Cell*, **65**, 241–248.

36. Zapp,M.L., Stern,S. and Green,M.R. (1993) Small molecules that selectively block RNA binding of HIV-1 Rev protein inhibit Rev function and viral production. *Cell*, **74**, 969–978.

37. Ratmeyer,L., Zapp,M.L., Green,M.R., Vinayak,R., Kumar,A., Boykin,D.W. and Wilson,W.D. (1996) Inhibition of HIV-1 Rev-RRE interaction by diphenylfuran derivatives. *Biochemistry*, **35**, 13689–13696.

38. Xiao,G., Kumar,A., Li,K., Rigl,C.T., Bajic,M., Davis,T.M., Boykin,D.W. and Wilson,W.D. (2001) Inhibition of the HIV-1 rev-RRE complex formation by unfused aromatic cations. *Bioorg. Med. Chem.*, **9**, 1097–1113.

39. Jin,Y. and Cowan,J.A. (2006) Targeted cleavage of HIV rev response element RNA by metallopeptide complexes. *J. Am. Chem. Soc.*, **128**, 410–411.

40. Prado,S., Beltran,M., Coiras,M., Bedoya,L.M., Alcami,J. and Gallego,J. (2016) Bioavailable inhibitors of HIV-1 RNA biogenesis identified through a Rev-based screen. *Biochem. Pharmacol.*, **107**, 14–28.

41. Rausch,J.W. and Le Grice,S.F. (2015) HIV rev assembly on the rev response element (RRE): A structural perspective. *Viruses*, **7**, 3053–3075.

42. Bai,Y., Tambe,A., Zhou,K. and Doudna,J.A. (2014) RNA-guided assembly of Rev-RRE nuclear export complexes. *eLife*, **3**, e03656.

43. Battiste,J.L., Tan,R., Frankel,A.D. and Williamson,J.R. (1994) Binding of an HIV Rev peptide to Rev responsive element RNA induces formation of purine-purine base pairs. *Biochemistry*, **33**, 2741–2747.

44. Peterson,R.D., Bartel,D.P., Szostak,J.W., Horvath,S.J. and Feigon,J. (1994) 1H NMR studies of the high-affinity Rev binding site of the Rev responsive element of HIV-1 mRNA: base pairing in the core binding element. *Biochemistry*, **33**, 5357–5366.

45. Mann,D.A., Mikaelian,I., Zemmel,R.W., Green,S.M., Lowe,A.D., Kimura,T., Singh,M., Butler,P.J., Gait,M.J. and Karn,J. (1994) A molecular rheostat. Co-operative rev binding to stem I of the rev-response element modulates human immunodeficiency virus type-1 late gene expression. *J. Mol. Biol.*, **241**, 193–207.

46. Kjems,J., Brown,M., Chang,D.D. and Sharp,P.A. (1991) Structural analysis of the interaction between the human immunodeficiency virus Rev protein and the Rev response element. *Proc. Natl. Acad. Sci. U.S.A.*, **88**, 683–687.

47. Kjems,J., Frankel,A.D. and Sharp,P.A. (1991) Specific regulation of mRNA splicing in vitro by a peptide from HIV-1 Rev. *Cell*, **67**, 169–178.

48. Daugherty,M.D., D'Orso,I. and Frankel,A.D. (2008) A solution to limited genomic capacity: using adaptable binding surfaces to assemble the functional HIV Rev oligomer on RNA. *Mol. Cell*, **31**, 824–834.

49. Zemmel,R.W., Kelley,A.C., Karn,J. and Butler,P.J. (1996) Flexible regions of RNA structure facilitate co-operative Rev assembly on the Rev-response element. *J. Mol. Biol.*, **258**, 763–777.

50. Pond,S.J., Ridgeway,W.K., Robertson,R., Wang,J. and Millar,D.P. (2009) HIV-1 Rev protein assembles on viral RNA one molecule at a time. *Proc. Natl. Acad. Sci. U.S.A.*, **106**, 1404–1408.

51. Daugherty,M.D., Booth,D.S., Jayaraman,B., Cheng,Y. and Frankel,A.D. (2010) HIV Rev response element (RRE) directs assembly of the Rev homooligomer into discrete asymmetric complexes. *Proc. Natl. Acad. Sci. U.S.A.*, **107**, 12481–12486.

52. Daugherty,M.D., Liu,B. and Frankel,A.D. (2010) Structural basis for cooperative RNA binding and export complex assembly by HIV Rev. *Nat. Struct. Mol. Biol.*, **17**, 1337–1342.

53. Fernandes,J., Jayaraman,B. and Frankel,A. (2012) The HIV-1 Rev response element: an RNA scaffold that directs the cooperative assembly of a homo-oligomeric ribonucleoprotein complex. *RNA Biol.*, **9**, 6–11.

54. Fang,X., Wang,J., O'Carroll,I.P., Mitchell,M., Zuo,X., Wang,Y., Yu,P., Liu,Y., Rausch,J.W., Dyba,M.A. *et al.* (2013) An unusual topological structure of the HIV-1 Rev response element. *Cell*, **155**, 594–605.

55. Sherpa,C., Rausch,J.W., Le Grice,S.F., Hammarskjold,M.L. and Rekosh,D. (2015) The HIV-1 Rev response element (RRE) adopts alternative conformations that promote different rates of virus replication. *Nucleic Acids Res.*, **43**, 4676–4686.

56. Jayaraman,B., Crosby,D.C., Homer,C., Ribeiro,I., Mavor,D. and Frankel,A.D. (2014) RNA-directed remodeling of the HIV-1 protein Rev orchestrates assembly of the Rev-Rev response element complex. *eLife*, **3**, e04120.

57. Van Ryk,D.I. and Venkatesan,S. (1999) Real-time kinetics of HIV-1 Rev-Rev response element interactions. Definition of minimal binding sites on RNA and protein and stoichiometric analysis. *J. Biol. Chem.*, **274**, 17452–17463.

58. Bartel,D.P., Zapp,M.L., Green,M.R. and Szostak,J.W. (1991) HIV-1 Rev regulation involves recognition of non-Watson-Crick base pairs in viral RNA. *Cell*, **67**, 529–536.

59. Huang,X.J., Hope,T.J., Bond,B.L., McDonald,D., Grahl,K. and Parslow,T.G. (1991) Minimal Rev-response element for type 1 human immunodeficiency virus. *J. Virol.*, **65**, 2131–2134.

60. Jain,C. and Belasco,J.G. (1996) A structural model for the HIV-1 Rev-RRE complex deduced from altered-specificity rev variants isolated by a rapid genetic strategy. *Cell*, **87**, 115–125.

61. Kjems,J., Calnan,B.J., Frankel,A.D. and Sharp,P.A. (1992) Specific binding of a basic peptide from HIV-1 Rev. *EMBO J.*, **11**, 1119–1129.

62. Battiste,J.L., Tan,R., Frankel,A.D. and Williamson,J.R. (1995) Assignment and modeling of the rev response element RNA bound to a Rev peptide using 13C-heteronuclear NMR. *J. Biomol. NMR*, **6**, 375–389.

63. Peterson,R.D. and Feigon,J. (1996) Structural change in Rev responsive element RNA of HIV-1 on binding Rev peptide. *J. Mol. Biol.*, **264**, 863–877.

64. Battiste,J.L., Mao,H., Rao,N.S., Tan,R., Muhandiram,D.R., Kay,L.E., Frankel,A.D. and Williamson,J.R. (1996) Alpha

helix-RNA major groove recognition in an HIV-1 rev peptide-RRE RNA complex. *Science*, **273**, 1547–1551.

65. Ippolito,J.A. and Steitz,T.A. (2000) The structure of the HIV-1 RRE high affinity rev binding site at 1.6 A resolution. *J. Mol. Biol.*, **295**, 711–717.

66. Hung,L.W., Holbrook,E.L. and Holbrook,S.R. (2000) The crystal structure of the Rev binding element of HIV-1 reveals novel base pairing and conformational variability. *Proc. Natl. Acad. Sci. U.S.A.*, **97**, 5107–5112.

67. Charpentier,B., Stutz,F. and Rosbash,M. (1997) A dynamic in vivo view of the HIV-I Rev-RRE interaction. *J. Mol. Biol.*, **266**, 950–962.

68. Tanamura,S., Terakado,H. and Harada,K. (2016) Cooperative dimerization of a stably folded protein directed by a flexible RNA in the assembly of the HIV Rev dimer-RRE stem II complex. *J. Mol. Recognit.*, **29**, 199–209.

69. Neuner,S., Santner,T., Kreutz,C. and Micura,R. (2015) The "Speedy" synthesis of Atom-Specific (15)N Imino/Amido-Labeled RNA. *Chemistry*, **21**, 11634–11643.

70. Delaglio,F., Grzesiek,S., Vuister,G.W., Zhu,G., Pfeifer,J. and Bax,A. (1995) NMRPipe: a multidimensional spectral processing system based on UNIX pipes. *J. Biomol. NMR*, **6**, 277–293.

71. Hansen,A.L., Nikolova,E.N., Casiano-Negroni,A. and Al-Hashimi,H.M. (2009) Extending the range of microsecond-to-millisecond chemical exchange detected in labeled and unlabeled nucleic acids by selective carbon R(1rho) NMR spectroscopy. *J. Am. Chem. Soc.*, **131**, 3818–3819.

72. Clay,M.C., Ganser,L.R., Merriman,D.K. and Al-Hashimi,H.M. (2017) Resolving sugar puckers in RNA excited states exposes slow modes of repuckering dynamics. *Nucleic Acids Res.*, **45**, e134.

73. Pervushin,K., Riek,R., Wider,G. and Wuthrich,K. (1997) Attenuated T-2 relaxation by mutual cancellation of dipole-dipole coupling and chemical shift anisotropy indicates an avenue to NMR structures of very large biological macromolecules in solution. *Proc. Natl. Acad. Sci. U.S.A.*, **94**, 12366–12371.

74. Kimsey,I.J., Petzold,K., Sathyamoorthy,B., Stein,Z.W. and Al-Hashimi,H.M. (2015) Visualizing transient Watson-Crick-like mispairs in DNA and RNA duplexes. *Nature*, **519**, 315–320.

75. Bothe,J.R., Stein,Z.W. and Al-Hashimi,H.M. (2014) Evaluating the uncertainty in exchange parameters determined from off-resonance R-1 rho relaxation dispersion for systems in fast exchange. *J. Magn. Reson.*, **244**, 18–29.

76. Wagenmakers,E.J. and Farrell,S. (2004) AIC model selection using Akaike weights. *Psychon. Bull. Rev.*, **11**, 192–196.

77. Burnham,K.P. and R.,A.D. (2004) Multimodel Inference: Understanding AIC and BIC in Model Selection. *Sociol. Methods Res.*, **33**, 261–304.

78. Luedtke,N.W. and Tor,Y. (2003) Fluorescence-based methods for evaluating the RNA affinity and specificity of HIV-1 Rev-RRE inhibitors. *Biopolymers*, **70**, 103–119.

79. Xue,Y., Kellogg,D., Kimsey,I.J., Sathyamoorthy,B., Stein,Z.W., McBrairty,M. and Al-Hashimi,H.M. (2015) Characterizing RNA Excited States Using NMR Relaxation Dispersion. *Methods Enzymol.*, **558**, 39–73.

80. Palmer,A.G. and Massi,F. (2006) Characterization of the dynamics of biomacromolecules using rotating-frame spin relaxation NMR spectroscopy. *Chem. Rev.*, **106**, 1700–1719.

81. Parisien,M. and Major,F. (2008) The MC-Fold and MC-Sym pipeline infers RNA structure from sequence data. *Nature*, **452**, 51–55.

82. Carbonnaux,C., van der Marel,G.A., van Boom,J.H., Guschlbauer,W. and Fazakerley,G.V. (1991) Solution structure of an oncogenic DNA duplex containing a G.A mismatch. *Biochemistry*, **30**, 5449–5458.

83. Brown,T., Hunter,W.N., Kneale,G. and Kennard,O. (1986) Molecular structure of the G.A base pair in DNA and its implications for the mechanism of transversion mutations. *Proc. Natl. Acad. Sci. U.S.A.*, **83**, 2402–2406.

84. Moroder,H., Kreutz,C., Lang,K., Serganov,A. and Micura,R. (2006) Synthesis, oxidation behavior, crystallization and structure of 2′-methylseleno guanosine containing RNAs. *J. Am. Chem. Soc.*, **128**, 9909–9918.

85. Brown,T., Leonard,G.A., Booth,E.D. and Kneale,G. (1990) Influence of pH on the conformation and stability of mismatch base-pairs in DNA. *J. Mol. Biol.*, **212**, 437–440.

86. Dorman,D.E. and Roberts,J.D. (1970) Nuclear magnetic resonance spectroscopy. C-13 spectra of some common nucleotides. *Proc. Natl. Acad. Sci. U.S.A.*, **65**, 19–26.

87. Lane,A.N. and Peck,B. (1995) Conformational flexibility in DNA duplexes containing single G.G mismatches. *Eur. J. Biochem.*, **230**, 1073–1087.

88. Tan,R., Chen,L., Buettner,J.A., Hudson,D. and Frankel,A.D. (1993) RNA recognition by an isolated alpha helix. *Cell*, **73**, 1031–1040.

89. Lea,W.A. and Simeonov,A. (2011) Fluorescence polarization assays in small molecule screening. *Expert Opin. Drug Discov.*, **6**, 17–32.

90. Hammond,J.A., Lamichhane,R., Millar,D.P. and Williamson,J.R. (2017) A DEAD-Box helicase mediates an RNA structural transition in the HIV-1 rev response element. *J. Mol. Biol.*, **429**, 697–714.

91. Tian,S. and Das,R. (2016) RNA structure through multidimensional chemical mapping. *Q. Rev. Biophys.*, **49**, e7.

92. Heaphy,S., Finch,J.T., Gait,M.J., Karn,J. and Singh,M. (1991) Human immunodeficiency virus type 1 regulator of virion expression, rev, forms nucleoprotein filaments after binding to a purine-rich "bubble" located within the rev-responsive region of viral mRNAs. *Proc. Natl. Acad. Sci. U.S.A.*, **88**, 7366–7370.

93. Iwai,S., Pritchard,C., Mann,D.A., Karn,J. and Gait,M.J. (1992) Recognition of the high affinity binding site in rev-response element RNA by the human immunodeficiency virus type-1 rev protein. *Nucleic Acids Res.*, **20**, 6465–6472.